Journal of Statistical Physics, Vol. 50, Nos. 5/6, 1988

Common Periodic Behavior in Larger and Larger Truncations of the Navier–Stokes Equations

Valter Franceschini,[1] Claudio Giberti,[1] and Marco Nicolini[1]

Received March 19, 1987

The periodic behavior of N-mode truncations of the Navier–Stokes equations on a two-dimensional torus is studied for $N = 44, 60, 80$, and 98. Significant common features are found, particularly for not too high Reynolds numbers. In all models periodicity ends, giving rise, though at quite different parameter values, to quasiperiodicity.

KEY WORDS: Fixed point; periodic orbit; limit behavior; bifurcation theory; truncated Navier–Stokes equations.

1. INTRODUCTION

A pioneering work by Lorenz[1] of 1963, concerning the Saltzman equations for convection between plates, represented the first attempt to study the partial differential equations that govern a fluid flow through truncation of a suitable Fourier expansion to a finite number of components ("modes"). Only 15 years later, and as a consequence of the rapid development of computers, other authors followed Lorentz in this line of research. Curry[2] investigated a 14-extension of the Lorentz model. Yahata[3] considered truncations up to 56 modes for the Taylor–Couette flow between concentric cylinders. Da Costa *et al.*[4] proposed a simplified model for the convection of a fluid in a layer with a dissolved solute. Boldrighini and Franceschini[5] began a series of detailed studies, strongly based on bifurcation theory, of truncations of the two-dimensional Navier–Stokes equations with periodic boundary conditions. Spectral

[1] Dipartimento di Matematica Pura ed Applicata, Università di Modena, 41100 Modena, Italy.

0022-4715/88/0300-0879$06.00/0

techniques were used by Orszag and co-workers to simulate, among other things, the three-dimensional Navier–Stokes equations associated with the plane Poiseuille and Couette flows[6] and the Taylor–Green vortex.[7] Maschke and Saramito[8] studied the transition to turbulence of a plasma confined in a magnetic field.

An extensive study of the Navier–Stokes equations on a two-dimensional torus was performed starting from Ref. 5. Several truncations were investigated in deep detail, from a minimal truncation with four modes[9] to a large one with 98 modes.[10] While for truncations up to 18 modes[11] the investigation concerned the whole sequence of successive bifurcations leading from a stationary regime to a chaotic one, for larger truncations it was confined to the stationary solutions only.

Two motivations were at the basis of this systematic study of truncated Navier–Stokes equations. The first motivation consisted in answering the following question: Is it really possible to study the Navier–Stokes equations through truncations? In other words: Is it possible to attain a qualitative limit behavior as the number N of modes used for the truncation is increased and with N not too large so that the numerical investigation can be carried out with acceptable computational costs? The second motivation lay in the assumption that truncated models could be very interesting as dynamical systems because they provide detailed descriptions of phenomena which qualitatively are the same as the ones often occurring in real world.

The results achieved from truncated Navier–Stokes equations widely justify these studies in the framework of dynamical systems. On the contrary, the answer to the question about the limit behavior is still partial. On one hand, in fact, if N is small (say, to fix ideas, $N \leqslant 20$), and the modes are arbitrarily chosen, even the addition or change of one mode can radically alter the phenomenology (see, for instance, Franceschini[12]). On the other hand, if the modes taken into account are all the ones included in a ball (which seems the most natural way of truncating), the first three nontrivial truncations, which correspond to $N = 12$, 14, and 18, show some common global features, but rather different details.[11] However, if one restricts the study to the fixed points only and considers larger and larger balls up to the one with 98 modes,[10] one sees that from $N = 44$ on the behavior does not undergo any qualitative change and, in addition, the critical parameter values at which the bifurcations take place tend to stabilize as N approaches 98.

We also note that interesting theoretical results, providing an estimate to the minimal number of modes necessary to obtain a correct approximate solution of the two-dimensional Navier–Stokes equations, were obtained by Foias *et al.*[13] Such estimates, however, are normally largely in excess

and, as seen by Maschke and Saramito[14] for the Rayleigh–Benard convection, do not appear very useful in view of actual applications.

With this paper we intend to give another contribution to answer the previous question. We consider in fact four of the truncations already considered in Ref. 10, the ones corresponding to $N = 44$, 60, 80, and 98, and thanks to a supercomputer CRAY X-MP, we investigate in detail the behavior of the periodic orbits present in the models. This allows us to show several common features, in some cases very striking, so that it makes sense to speak about a good limit behavior of the periodic orbits, at least for the Reynolds number R not too large.

In regard to the techniques we use in the numerical investigation, besides the fundamental support of bifurcation theory (see, for instance, Iooss and Joseph[15]), our main tool is a quasi-Newton method, Broyden's method, to identify and follow periodic orbits. A special Appendix is devoted to the discussion of the numerical methods and of the arrangements adopted to optimize the programming on the vector computer CRAY X-MP we used for the computations. We remark that the setting up of our programs, in view of optimizing the performance of the computer, required a lot work, which prompted us to discuss, though briefly, the argument.

The paper is organized as follows. In Section 2 we introduce the truncated models and describe their properties. In Section 3 we report the behavior of the stationary solutions. In Section 4, which contains the original results of this work, we illustrate in detail the periodic orbit behavior, with the help of pictures for better clearness. Finally, in Section 5 we make some conclusive remarks.

2. THE TRUNCATED EQUATIONS

Let L be a finite set of $2N$ wave vectors $\mathbf{k}$ with integer components (k_x, k_y) such that if $\mathbf{k} \in L$, also $-\mathbf{k} \in L$. An N-mode truncation of the Navier–Stokes equations for an incompressible fluid on a two-dimensional torus is defined as

$$\begin{aligned} \dot{\gamma}_{\mathbf{k}} &= -\nu |\mathbf{k}|^2 \gamma_{\mathbf{k}} - i \sum_{\substack{\mathbf{k}_1 + \mathbf{k}_2 + \mathbf{k} = 0 \\ \mathbf{k}_1, \mathbf{k}_2 \in L}} \frac{(\mathbf{k}_1^{\perp} \cdot \mathbf{k}_2)(k_2^2 - k_1^2)}{2 |\mathbf{k}_1| \, |\mathbf{k}_2| \, |\mathbf{k}|} \bar{\gamma}_{\mathbf{k}_1} \bar{\gamma}_{\mathbf{k}_2} + f_{\mathbf{k}} \\ \gamma_{-\mathbf{k}} &= -\bar{\gamma}_{\mathbf{k}}, \qquad \mathbf{k} \in L \end{aligned} \tag{1}$$

where $\gamma_{\mathbf{k}}$ is the component along $\mathbf{k}^{\perp} = (k_y, -k_x)$ of the velocity field $\mathbf{u}$, f_k is the analogous component of the external periodic force $\mathbf{f}$ driving the fluid, and ν is the viscosity.

System (1) consists of N ordinary differential equations in the complex unknowns $\gamma_{\mathbf{k}}(t)$, which implies $2N$ equations in real variables. We shall refer only to the $\mathbf{k}$'s placed in the half-space

$$\Pi^+ = \{(x, y), x > 0\} \cup \{(0, y), y > 0\}$$

Then, for the sake of simplicity, we assume that the force $\mathbf{f}$ acts only on some mode $\mathbf{k}^*$ and is independent of time. Under these hypotheses $\mathbf{f}_{\mathbf{k}^*}$ can be taken real without losing generality. As a consequence, system (1) admits "particular" solutions in which each $\gamma_{\mathbf{k}}(t)$ is either real or pure imaginary. To consider such a solution allows the study of a system of N rather than $2N$ equations.

To proceed in agreement with the notations of previous works, let $L^{(M)}$ be the set of modes $\mathbf{k}$ such that $|\mathbf{k}|^2 = k_x^2 + k_y^2 \leqslant M$, with M the sum of two squared integers, and let $S^{(M)}$ be the truncation associated with $L^{(M)}$. As the "balls" of radius $\sqrt{M}$ become larger and larger, the truncations $S^{(M)}$ provide a sequence of models, each of them representing an enlargement of all the previous ones. Furthermore, let the $\mathbf{k}$'s be ordered for increasing modulus and, in the case of equality, for decreasing k_y. Then, $\mathbf{k}_1 = (0, 1)$, $\mathbf{k}_2 = (1, 0)$, $\mathbf{k}_3 = (1, 1)$, $\mathbf{k}_4 = (1, -1)$, and so on. Now, after taking $\mathbf{k}^* \equiv \mathbf{k}_9 = (2, -1)$ and letting $R = f_9$, we can assume $\nu = 1$ by rescaling the equations in length and time. Hence, the external parameter R can be referred to as the Reynolds number.

In order or define the models to be studied, we need first to make precise the meaning of a "particular" solution and then to say which "particular" solution we adopt. Under the above assumptions, there exist infinitely many hyperplanes, subspaces of the $2N$-dimensional phase space, which are invariant with respect to the flow defined by system (1). These hyperplanes are symmetric due to a one-parameter group of angular symmetries. In fact, writing $\gamma_{\mathbf{k}}(t)$ in the polar form

$$\gamma_{\mathbf{k}}(t) = \rho_{\mathbf{k}}(t) \exp[i\theta_{\mathbf{k}}(t)]$$

with both $\rho_{\mathbf{k}}(t)$ and $\theta_{\mathbf{k}}(t)$ varying in $(-\infty, +\infty)$, if α and β are real parameters, $\alpha \in [0, 2\pi)$, $\beta \in [0, \pi)$, then

$$S_\alpha: \quad \{\theta_{\mathbf{k}}(t) \to \theta_{\mathbf{k}}(t) + (k_x + 2k_y)\alpha\}_{\mathbf{k} \in L^{(M)} \cap \Pi^+}$$

and

$$H_\beta: \quad \{\theta_{\mathbf{k}} = (k_x + 2k_y)\,\beta + (1 - k_x - k_y)\pi/2\}_{\mathbf{k} \in L^{(M)} \cap \Pi^+}$$

represent a one-parameter group of symmetries and a linear continuum of stationary solutions for $\{\theta_{\mathbf{k}}(t)\}_{\mathbf{k} \in L^{(M)} \cap \Pi^+}$ respectively. A "particular"

solution corresponds to the hyperplane H_0 or, equivalently, to $H_{\pi/2}$. We shall study the one associated with $H_{\pi/2}$, which means confining the choice of the initial conditions for (1) to the points of that hyperplane.

The adoption of a particular solution allows us to handle a reduced system of N equations in real variables $x_{\mathbf{k}}(t)$, for $\mathbf{k} \in L^{(M)} \cap \Pi^+$. This system is invariant with respect to the symmetry

$$T: \quad \{x_{\mathbf{k}} \to (-1)^{k_x} x_{\mathbf{k}}\}_{\mathbf{k} \in L^{(M)} \cap \Pi^+}$$

In addition, there exists a pseudosymmetry,

$$\tau: \quad \{x_{\mathbf{k}} \to (-1)^{k_x/2 + k_y} x_{\mathbf{k}}\}_{\mathbf{k} \in L^{(M)} \cap \Pi^+}$$

which works when all the variables $x_{\mathbf{k}}$ relative to $\mathbf{k}$'s with odd k_x are always null. While the knowledge of T is essential to an understanding of the whole behavior of our models, that of τ is necessary, as we shall see later, only to an understanding of the bifurcation diagram of the fixed points.

Here we consider the models $S^{(26)}$, $S^{(37)}$, $S^{(50)}$, and $S^{(64)}$, which correspond to $N = 44$, 60, 80, and 98, respectively. To give an idea about the dimension of the systems we are dealing with, we note that while $S^{(26)}$ consists of about 1000 nonlinear terms, $S^{(64)}$ has more than 5200 of them. We recall that a complete study of $S^{(8)}$, $S^{(9)}$, and $S^{(10)}$, i.e., the first three nontrivial truncations, has been performed in Ref. 11, while the subsequent models, up to $S^{(64)}$, have been investigated in Ref. 10, but only with regard to the stationary solutions. The reader is referred to these references and to Ref. 16 for more details on the arguments of this section.

3. THE STATIONARY SOLUTIONS

Three different sets of fixed points are present in the systems $S^{(M)}$. To distinguish them, we shall make use of the three letters P, Q, and O. While the points P and Q were studied in Ref. 10, the points O are discovered and then investigated here. In contrast to the first two families of points, which exist in all the $S^{(M)}$, the O family is found only for $M \geqslant 18$.

The fixed-point behavior, which is qualitatively the same in all the models $S^{(M)}$ for $M \geqslant 26$ (that is why we consider $S^{(26)}$ and larger truncations), is summarized in Fig. 1. Let us illustrate such behavior, a family of points at a time.

Points P. The only fixed point present for every value of R is P_0, which has all the components zero except for x_9, the component associated with the mode excited by the external force. P_0 loses stability at R_1 because

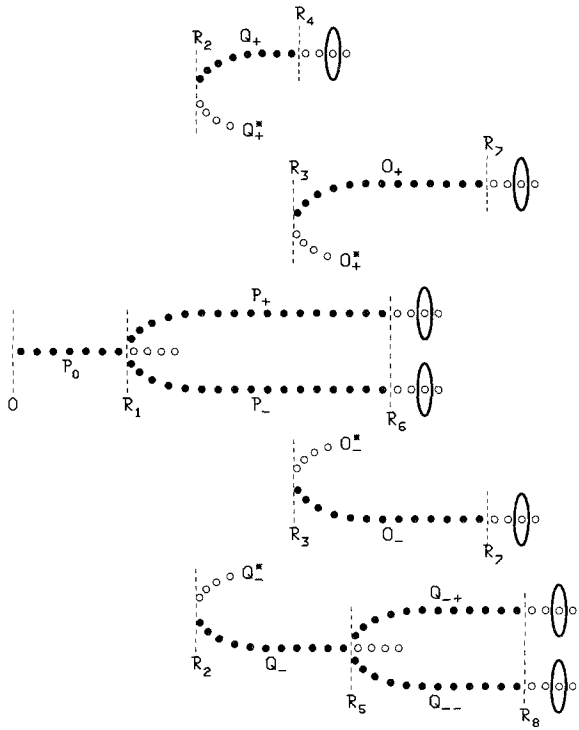

Fig. 1. Bifurcation diagram of the fixed points for the truncations $S^{(M)}$ for $M \geqslant 26$. Full circles represent stable fixed points, empty circles unstable ones, and ellipses stable periodic orbits.

of a real eigenvalue of the Jacobian of $S^{(M)}$, which becomes positive. The bifurcation causes a pair of new points P_γ, $\gamma = \pm$, to arise from P_0, which are stable and mutual images under the symmetry T. The P_γ, which have coordinates zero except for those relative to $\mathbf{k}$'s with the difference $(k_x - k_y)$ a multiple of three, keep stability up to R_6 when a pair of complex conjugate eigenvalues crosses the imaginary axis from left to right. A direct Hopf bifurcation takes place and two stable T-symmetric periodic orbits $H(P_\gamma)$ are generated from the P_γ.

Points Q. Two points (Q_δ, Q_δ^*) of fixed points, $\delta = \pm$, appear at R_2 in consequence of a saddle-node bifurcation. The points Q_δ and Q_δ^*, the former stable and the latter unstable, have coordinates $x_\mathbf{k}$ which are zero corresponding to $\mathbf{k}$'s with odd k_x. The pseudosymmetry τ holds and the Q_δ are changed into each other under application of τ, as well as the Q_δ^*. However, they undergo different behavior. Obviously, we are interested in that of the stable points.

Q_+ becomes unstable at R_4 due to a direct Hopf bifurcation. We call $H(Q_+)$ the stable T-invariant periodic orbit that originates from Q_+.

On the other hand, the behavior of Q_- is analogous to that of P_0. In fact, first Q_- bifurcates at R_5 into a pair of stable T-symmetric points $Q_{-\gamma}$, $\gamma = \pm$, then these lose stability at R_8 because of another direct Hopf bifurcation. Let $H(Q_{-\gamma})$ be the two stable T-symmetric periodic orbits appearing from the $Q_{-\gamma}$.

Points O. Two extra pairs (O_γ, O_γ^*) of fixed points, $\gamma = \pm$, O_γ stable and O_γ^* unstable, arise via a saddle-node bifurcation at R_3. The O_γ (as well as the O_γ^*) are T-symmetric, so that they behave in the same way and analogously to Q_+. Each O_γ, in fact, becomes unstable due to a further direct Hopf bifurcation that occurs at R_7 and gives rise to a stable periodic orbit $H(O_\gamma)$.

Table I reports the numerical values of the bifurcation points R_i, $i = 1,..., 8$, which describe the behavior of the stationary solutions in the models considered here. Except for R_3 and R_7, they are taken (and reordered) from the analogous table of Ref. 10.

4. THE PERIODIC SOLUTIONS

Consider then the periodic solutions of $S^{(26)}$, $S^{(37)}$, $S^{(50)}$, and $S^{(64)}$. As we have just seen, they exhibit four distinct Hopf bifurcations, which lead successively to the appearance of the periodic orbits $H(Q_+)$, $H(P_\gamma)$, $H(O_\gamma)$, and $H(Q_{-\gamma})$. In addition, we discovered, through direct integration of the equations, that an extra periodic orbit K is present in all four models. We shall describe separately the behavior of each of these orbits, excluding only $H(Q_+)$. The exclusion is due to a rather large period (and then to high computational costs) on one hand, and to an apparently small basin of attraction (and then to scant importance for the dynamics) on the other.

Orbits $H(P_\gamma)$. The behavior of these orbits in the four models is exactly the same: they remain stable until they disappear via a saddle-node

Table I

M	N	R_1	R_2	R_3	R_4	R_5	R_6	R_7	R_8
26	44	19.78	31.71	48.76	50.01	57.18	64.28	78.38	87.79
37	60	19.78	31.53	48.23	49.23	57.23	65.49	82.82	88.21
50	80	19.78	31.58	48.49	49.30	58.86	65.31	82.02	87.37
64	98	19.77	31.58	48.46	49.45	58.62	65.37	81.87	87.96

bifurcation. The approximated critical values of the Reynolds number R for which the bifurcation occurs in $S^{(26)}$, $S^{(37)}$, $S^{(50)}$, and $S^{(64)}$ are 75.97, 82.79, 78.84, and 80.16, respectively. In all cases we verified the existence of an unstable periodic orbit in a neighborhood of H (P_γ), tending to collapse onto it as R approaches the bifurcation point.

Orbits $H(O_\gamma)$. These periodic orbits behave identically only in the three largest systems. Let us describe such behavior, omitting for the moment what happens in $S^{(26)}$. Each $H(O_\gamma)$ becomes unstable due to a period-doubling bifurcation, which causes a stable periodic orbit with double period to arise. By following the bifurcated orbit, we could verify that it also undergoes a bifurcation of the same kind. It is reasonable to hypothesize that the sequence of bifurcations is actually infinite. Concerning the numerical values of the parameter R at the critical points, we found that the first doubling occurs at $R \simeq 97.06$ for $M = 37$, $R \simeq 91.45$ for $M = 50$, and $R \simeq 91.30$ for $M = 64$, while the second doublings take place at $R \simeq 106.25$, $R \simeq 98.23$, and $R \simeq 98.41$, respectively.

As for the system $S^{(26)}$, also here $H(O_\gamma)$ loses stability because of a real eigenvalue of the Jacobian of the Poincaré map leaving the unit circle through -1. In this case, however, no stable periodic orbit with double period seems to be present after the bifurcation has occurred.

Orbits K. While the other periodic orbits arise from fixed points via Hopf bifurcation, and then they represent a natural continuation of already known situations, the orbits K can be found only by integrating the equations $S^{(M)}$ with randomly chosen initial data and for proper values of the Reynolds number R. For $R = 110$, for instance, an orbit K, invariant under application of the symmetry T, exists in all four models (see Fig. 2) and is easy to find. Let us illustrate its behavior starting from the lowest truncation.

In $S^{(26)}$ the orbit K is originated by a a saddle-node bifurcation occurring at $R \simeq 91.61$. As R is increased, K loses stability at $R \simeq 128.14$ because a real eigenvalue of the Jacobian of the Poincaré map crosses the unit circle through $+1$. Several attempts to verify a direct symmetry-breaking bifurcation, i.e., the presence of two stable T-symmetric orbits K_1 and K_2 in a neighborhood of K just after the bifurcation has occurred, were useless. Perhaps the bifurcation is subcritical.

Concerning the system $S^{(37)}$, K arises again in consequence of a saddle-node bifurcation taking place at $R \simeq 98.45$. Now, however, it is easy to check that a direct symmetry-breaking bifurcation occurs as the Reynolds number R is increased toward $R \simeq 122.61$. The bifurcated orbits K_1 and K_2, stable and symmetrically placed with respect to K, become unstable at $R \simeq 128.22$ due to a period-doubling bifurcation. In turn, the

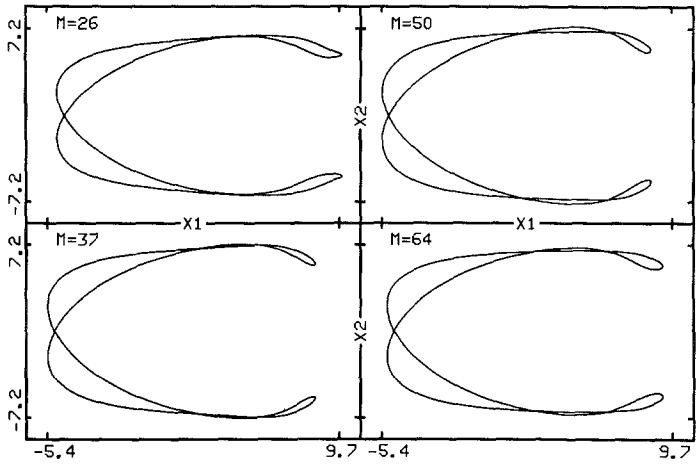

Fig. 2. The (x_1, x_2) projection of the periodic orbit K for $R = 110$ and $M = 26, 37, 50,$ and 64.

stable doubled orbits originating from K_1 and K_2 undergo a bifurcation of the same kind at $R \simeq 128.95$. We hypothesize a sequence of infinitely many doublings.

Finally, consider the behavior of K in $S^{(50)}$ and $S^{(64)}$, where it turns out to be the same. As R is increased, the phenomenology repeats exactly that in $S^{(37)}$. In fact, first K undergoes a symmetry-breaking bifurcation, then the bifurcated orbits K_1 and K_2 give rise to a sequence, presumably infinite, of period doublings. The approximate critical values of R associated with the symmetry breaking and with two doublings are respectively 126.13, 128.03, and 128.26 for $S^{(50)}$ and 120.14, 124.87, and 125.11 for $S^{(64)}$. On the other hand, following K as R is decreased, instead of finding a saddle-node bifurcation as for $S^{(26)}$ and $S^{(37)}$, one finds a symmetry breaking followed by a period doubling. In other words, now the behavior of K in both directions of the parameter R is the same. The symmetry breaking and the first doubling occur at $R \simeq 90.605$ and $R \simeq 90.527$ in the case of $S^{(50)}$ and $R \simeq 91.782$ and $R \simeq 91.712$ in the case of $S^{(64)}$.

Figure 2 and further analogous pictures show a very striking similarity among the orbits K in the four truncations we are considering. This provides evidence of a good stabilization, also from a quantitative point of view, of the periodic behavior associated with these orbits.

Orbits $H(Q_{-\gamma})$. We left the description of these periodic orbits last because they are just the ones that disappear last. In contrast to the previous orbits, the $H(Q_{-\gamma})$ are present in a quite wide range of the parameter R. This range is sensibly different from a truncation to another.

In spite of this and in spite of different bifurcations, all the $H(Q_{-\gamma})$ become unstable, giving rise to an attracting torus. This allows us to state that, from a qualitative point of view, the behavior of the $H(Q_{-\gamma})$ is substantially the same in the four models we are dealing with.

As far as $S^{(26)}$ and $S^{(37)}$ are concerned, each $H(Q_{-\gamma})$ keeps stability until a pair of complex conjugate eigenvalues of the Jacobian of the Poincaré map, at $R \simeq 251.98$ and $R \simeq 561.54$ respectively, escapes from the unit circle. By making a Poincaré section of the flow for a value of R a little far from the bifurcation point, it is easy to verify that in both cases a two-dimensional torus has appeared.

Coming to the behavior of $H(Q_{-\gamma})$ in $S^{(50)}$, it turns out to be a little involved. A period-doubling bifurcation takes place at $R \simeq 179.79$, making $H(Q_{-\gamma})$ unstable and generating a stable orbit with double period. This new orbit persists up to $R \simeq 301.59$ and in this wide parameter range seems to be the only attractor present. The double orbit disappears by collapsing again onto $H(Q_{-\gamma})$, so returning stability to it. This is a direct period-doubling bifurcation taking place for reverse R. The story of the life of $H(Q_{-\gamma})$ goes to an end because of a saddle-node bifurcation occurring at $R = R'' \simeq 303.91$, where it collapses, disappearing with a neighboring unstable orbit. This orbit was born a little before, via another saddle-node bifurcation at $R = R' \simeq 302.44$, together with a stable orbit very similar in shape to $H(Q_{-\gamma})$. This stable orbit coexists with $H(Q_{-\gamma})$ in the interval (R', R'') and in practice takes the place of $H(Q_{-\gamma})$ for $R > R''$. For this reason we refer to this new orbit still as $H(Q_{-\gamma})$. Then the story continues and for a long time. In fact the orbit remains stable up to $R \simeq 540.20$,

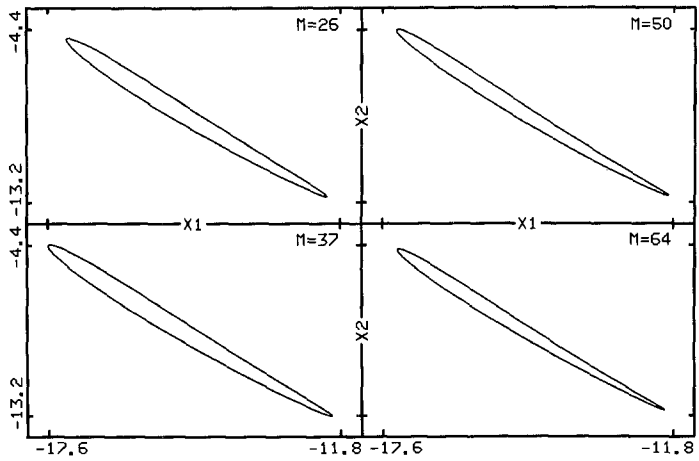

Fig. 3. The (x_1, x_2) projection of the periodic orbit $H(Q_{-\gamma})$ for $R = 170$ and $M = 26$, 37, 50, and 64.

where we have numerical evidence of a bifurcation into an attracting two-dimensional torus.

Finally, consider what happens to the orbit $H(Q_{-\gamma})$ in the system $S^{(64)}$. While no period doubling occurs, the previous phenomenology associated with a couple of successive saddle-node bifurcations is present. In fact, first at $R = R' \simeq 420.4$ a pair of stable–unstable new periodic orbits arises with shape analogous to $H(Q_{-\gamma})$, then the unstable orbit collapse onto $H(Q_{-\gamma})$, disappearing with it at $R = R'' \simeq 422.0$. The remaining orbit, which also in this case is regarded as $H(Q_{-\gamma})$, bifurcates into an attracting torus at $R \simeq 432.8$.

Figures 3 and 4 represent two different plane projections of the four orbits $H(Q_{-\gamma})$ that correspond to $R = 170$. We note that, while the projection onto the plane (x_1, x_2) shows four closed, very similar orbits, the projection onto (x_9, x_5) gives evidence of the fact that some differences still characterize the range of variableness of certain coordinates.

To complete the description of the periodic solutions of the models $S^{(26)}$, $S^{(37)}$, $S^{(50)}$, and $S^{(64)}$, we provide two pictures which allow an overall glance at the behaviors we have been discussing. Figure 5 shows in fact a graphical summary relative to the R interval (50, 200), while Fig. 6 concerns the R interval (200, 600), where only the orbits $H(Q_{-\gamma})$ are present.

5. CONCLUSION

We have presented the results of a study of the periodic solutions exhibited by four truncations, to 44, 60, 80, and 98 modes respectively, of

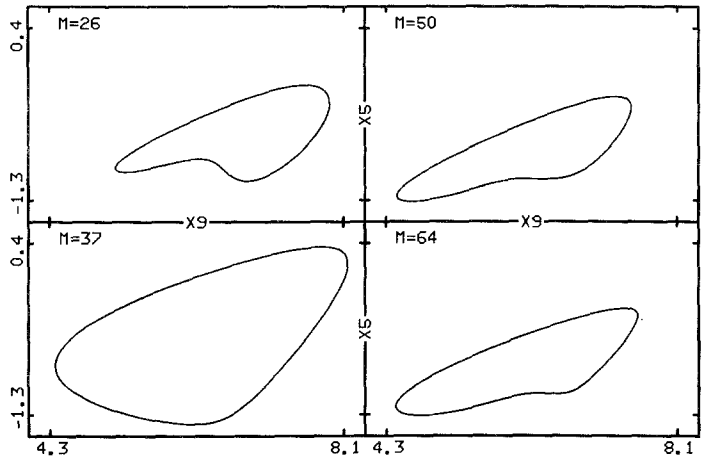

Fig. 4. The same orbits as Fig. 3, projected onto the plane (x_9, x_5).

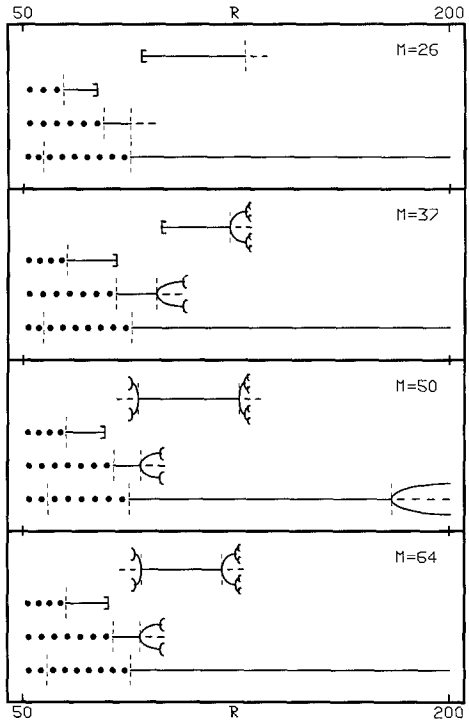

Fig. 5. Scale drawing summarizing the phenomenology of the four systems $S^{(26)}$, $S^{(37}$, $S^{(50)}$, and $S^{(64)}$ for R varying in the interval (50, 200). Each of the four parts of the picture corresponds to one of the systems and represents, from the top downward, first K_γ, then P_γ and $H(P_\gamma)$, then O_γ and $H(O_\gamma)$, and, at bottom, Q_-, $Q_{-\gamma}$, and $H(Q_{-\gamma})$. Full circles indicate stable fixed points, continuous and broken lines represent stable and unstable periodic orbits, respectively. A bracket is the symbol for a saddle-node bifurcation. A "pitchfork" represents either a period doubling or.a symmetry breaking.

the Navier–Stokes equations on a two-dimensional torus. The study, intended as the continuation of a previous work[10] concerning the stationary solutions, had the object of showing, also for the periodic solutions, some kind of limit behavior as the number of modes used in the truncation is increased. Figure 5, with the addition of Figs. 2–4, shows the attainment of the object, beyond any expected extent, in a wide range of the Reynolds number R. However, as was to be expected, as R is increased, things get worse (see Fig. 6), and a larger number of modes appears to be necessary in order to obtain more stabilized behavior.

The present results show that it is possible to analyze in deep detail systems of first-order ordinary differential equations with up to 100 equations. In this regard, however, it must be said that this limit is not easy

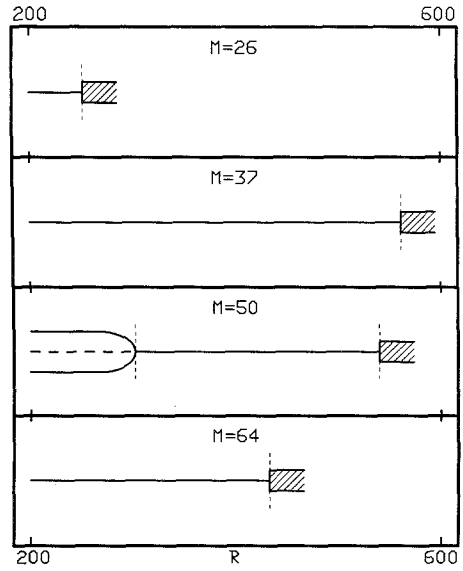

Fig. 6. Scale drawing representing the behavior of the periodic orbit $H(Q_{-\gamma})$, until it bifurcates into an attracting torus, in the R interval (200, 600). The two saddle-node bifurcations that occur in this parameter range in $S^{(50)}$ and $S^{(64)}$ are not "visible" at the scale of the picture.

to exceed in a substantial way. In fact, once we implemented the programs, we needed about 15 hr of computational time on the CRAY X-MP.

To conclude, we remark that it would be interesting to investigate the systems $S^{(M)}$ further. Two questions, in particular, appear worth answering: (1) Do the sequences of period doublings give rise to a strange attractor persisting, and then coexising with stable periodic orbits, as M is increased? (2) How does the transition to chaos occur from two-dimensional tori?

APPENDIX. NUMERICAL METHODS AND TECHNIQUES

In this Appendix we discuss the numerical problem of the investigation of a dissipative system of first-order nonlinear differential equations. As a matter of fact, this problem has already been treated more than once (see, for instance, Ref. 17). Here, however, we discuss, for the first time to our knowledge, two elements that we consider very important for the study of high-dimensional systems: the use of Broyden's method to find a periodic orbit and the techniques used to optimize the programming on the CRAY X-MP. We remark that they are not trivial arguments: the adoption of Broyden's method, implemented in an optimized way, can lead to

reduced computational time to at least one-third. We have tried to make this Appendix concise and at the same time self-explanatory.

Consider an autonomous equation, depending on one external parameter μ:

$$\dot{\mathbf{x}}(t) = \mathbf{F}(\mathbf{x}(t); \mu), \qquad \mathbf{x} \in R^N, \quad \mu \in R \tag{A.1}$$

or, more extensively,

$$\dot{x}_i(t) = F_i(x_1(t), x_2(t), \ldots, x_N(t); \mu), \qquad i = 1, \ldots, N$$

Let $\mathbf{\Phi}^t(\mathbf{x}_0, \mu)$ be its solution at time t when the initial condition is $\mathbf{x}(0) = \mathbf{x}_0$.

A *periodic* (or *closed*) *orbit* $\gamma(\mu)$ is a nonconstant solution of (A.1) with the property that there exists T, $0 < T < \infty$, such that, if $\mathbf{x}_0 \in \gamma(\mu)$, then $\mathbf{\Phi}^T(\mathbf{x}_0, \mu) = \mathbf{x}_0$. The minimal T is the period of the orbit. A periodic orbit γ can be then determined by looking for a solution $(\mathbf{x}^*, T)$ of the fixed-point equation

$$\mathbf{G}(\mathbf{x}, t) = \mathbf{\Phi}^t(\mathbf{x}) - \mathbf{x} = 0, \qquad \mathbf{x} \in R^N \tag{A.2}$$

where μ, which is fixed, is omitted.

A method to solve (A.2) is the Newton method. Its application leads to the following iterative procedure:

$$[W(\mathbf{x}_k, \tau_k) - I]\boldsymbol{\varepsilon}_k + \mathbf{F}(\mathbf{\Phi}^{\tau_k}(\mathbf{x}_k))\delta_k = \mathbf{x}_k - \mathbf{\Phi}^{\tau_k}(\mathbf{x}_k), \qquad k = 0, 1, \ldots \tag{A.3}$$

where $W(\mathbf{x}_k, \tau_k)$ (abbreviated W_k) is the $N \times N$ matrix of the first derivatives of the flow $\mathbf{\Phi}^t$ with respect to the spatial coordinates, I is the unit matrix, $\boldsymbol{\varepsilon}_k = \mathbf{x}_{k+1} - \mathbf{x}_k$, and $\delta_k = \tau_{k+1} - \tau_k$. Given an initial approximation $(\mathbf{x}_0, \tau_0)$, if the iteration (A.3) converges, the sequence $\{\mathbf{x}_k\}$ tends to some point $\mathbf{x}^*$ of a periodic orbit and the sequence $\{\tau_k\}$ tends to its period (or a multiple of it). Then, once we know (or suppose) that a closed orbit γ exists, if $\mathbf{x}_0$ is a point sufficiently close to γ and τ_0 is a sufficiently good approximation of its period, we can determine the orbit precisely.

For each k, (A.3) is a linear system of N equations in $N+1$ unknowns, the N components $\varepsilon_k^{(i)}$ of $\boldsymbol{\varepsilon}_k$ and δ_k. In order to solve it we can impose that one of the $\varepsilon_k^{(i)}$, say $\varepsilon_k^{(h)}$, is zero. This way we obtain a system of N equations in N unknowns, which can be rewritten in the simpler form

$$B_k \boldsymbol{\xi}_k = -\mathbf{G}(\mathbf{x}_k), \qquad k = 0, 1, \ldots \tag{A.4}$$

where $\boldsymbol{\xi}_k = (\varepsilon_k^{(1)}, \ldots, \varepsilon_k^{(h-1)}, \delta_k, \varepsilon_k^{(h+1)}, \ldots, \varepsilon_k^{(N)})$ and B_k coincides with $W_k - I$ except for the hth column, which is given by $\mathbf{F}(\mathbf{\Phi}^{\tau_k}(\mathbf{x}_k))$. If σ is the

accuracy that we require for the closure of the orbit, the iteration is stopped when the condition $\|\xi_{k+1} - \xi_k\| < \sigma$ is satisfied.

Broyden's method[18] maintains the iteration (A.4), but with B_k obtained from B_{k-1} in the following way:

$$B_{k+1} = B_k + \frac{(\mathbf{Y}_k - B_k \xi_k)\xi_k^T}{\xi_k^T \xi_k}, \qquad \mathbf{k} = 0, 1, \ldots \tag{A.5}$$

where $\mathbf{Y}_k = \mathbf{G}(\mathbf{x}_{k+1}, \tau_{k+1}) - \mathbf{G}(\mathbf{x}_k, \tau_k)$ and ξ_k^T is the transpose of ξ_k. We notice that, in contrast to Newton's method, Broyden's method requires one computation of W_k (to provide B_0). After starting, only the computation of $\mathbf{\Phi}^{\tau_{k+1}}(\mathbf{x}_{k+1})$ is needed to derive B_{k+1} from B_k, $k = 0, 1, \ldots$.

For both Newton's and Broyden's methods the main problem, as far as cost is concerned, is associated with the computation of W_k. There are two different methods to perform it.

Method 1. W_k is given by the solution at time τ_k of the $N \times N$ system of linear differential equations

$$\dot{W}(t) = J(t)\, W(t), \qquad W(0) = I \tag{A.6}$$

where $J(t)$ is the Jacobian of $\mathbf{F}$ computed at $\mathbf{\Phi}^t(\mathbf{x})$. We note that this system and system (A.1) must be integrated simultaneously.

Method 2. The jth column of W_k contains the derivative of $\mathbf{\Phi}^t$ with respect to x_j computed at (x_k, τ_k). So W_k can be approximated numerically by taking

$$(W_k)_{ij} = \left(\frac{\mathbf{\Phi}^{\tau_k}(\mathbf{y}_k^j) - \mathbf{\Phi}^{\tau_k}(\mathbf{x}_k)}{\Delta x} \right)_i \tag{A.7}$$

where $\mathbf{y}_k^j$ has the same coordinates as $\mathbf{x}_k$ except for the jth one, which is incremented by a conveniently small amount Δx. In this case we note that the computation of N trajectories is necessary.

There exists an alternative way of finding a periodic orbit. Such a method, which is based on the search of a fixed point of the Poincaré map, is completely analogous to, though a little more expensive than, the one we have described. The interested reader is referred to Ref. 17, where also the way of taking advantage of a symmetry of the orbit is illustrated.

Several arrangements, most of them introduced by Giberti,[19] were adopted in order to optimize the programming by taking into account the characteristics of the vector computer CRAY X-MP. We discuss some of them.

The first considerations concern the computation of the function $\mathbf{F}(\mathbf{x})$ in (A.1). In our case $\mathbf{F}$ is given by the system (1), which has the following quadratic form:

$$F_i = a_i x_i + \sum_{j=1}^{N} \sum_{k=1}^{N} b_{ijk} x_j x_k + r_i, \qquad i = 1,..., N$$

where the matrices $B_i = (b_{ijk})_{j,k=1,...,N}$ have most elements zero. Hence, it is convenient to rewrite the above sum only considering the nonzero elements:

$$F_i = a_i x_i + \sum_{l=1}^{M_i} c_{il} x_{j_{il}} x_{k_{il}} + r_i, \qquad i = 1,..., N \tag{A.8}$$

with $M_i < N$ for all i.

This formulation of $\mathbf{F}$, however, presents a considerable drawback: the x's are indirectly addressed, which prevents vectorizing. The best expedient to get out of this trouble is to construct a suitable vector $\mathbf{y}$ carrying the x_i in such a way that (A.8) becomes

$$F_i = a_i x_i + \sum_{l=1}^{M_i} c_{il}\, y_{2(L_i+l)-1}\, y_{2(L_i+l)} + r_i, \qquad i = 1,..., N \tag{A.9}$$

where $L_i = \sum_{k=1}^{i-1} M_k$. This final formulation of $\mathbf{F}$ is based on the existence of a library routine, the GATHER, which optimizes the construction of $\mathbf{y}$, and on the fact that the larger N is, the more efficient the routine is.

The second argument we discuss pertains the computation of W_k. Consider first Method 1. In this case the main question concerns the computation of the function $J(t)\, W(t)$ and, in particular, of $J(t)$. The Jacobian $J(t)$ at $\mathbf{x}(t)$ may be obtained in the following way after constructing four suitable matrices D_1, D_2, $Y_1(t)$, and $Y_2(t)$:

$$(J(t))_{ij} = (D_1)_{ij} (Y_1(t))_{ij} + (D_2)_{ij} (Y_2(t))_{ij}$$

D_1 and D_2 depend only on the coefficients a_i and c_{il},, while $Y_1(t)$ and $Y_2(t)$ depend only on $\mathbf{x}(t)$. It is possible to express $J(t)$ in this manner because in each scalar equation each x_l does not appear more than twice (which is, obviously, a peculiarity of the systems we are dealing with). We remark that such a split of $J(t)$ into the sum of two "products" of matrices is very convenient from a vector point of view. We also notice that the construction of the matrices Y_1 and Y_2 again implies overcoming a problem of indirect addressing, also in this case by calls, one for each matrix, to the routine GATHER.

As far as Method 2 is concerned, the best technique consists in

integrating simultaneously the $M = N + 1$ trajectories $\mathbf{\Phi}^{\tau_k}(\mathbf{x}_k)$ and $\mathbf{\Phi}^{\tau_k}(\mathbf{y}_k^i)$, $i = 1,..., N$. The parallel computation can be easily performed through the equation $\dot{\mathbf{X}} = \mathbf{G}(\mathbf{X})$, by $N \times M$ scalar equations, obtained by considering the direct product[20] of M copies of our Eq. (A.1), with the initial condition $\mathbf{X} = (\mathbf{x}_k, \mathbf{y}_k^1,..., \mathbf{y}_k^N)$. In this case, however, it is more convenient to arrange the computation vertically rather than horizontally [as for (A.9)].

While Methods 1 and 2 are comparable as for precision, Method 1 is surely better than Method 2 from the cost point of view. In fact, for $N = 44$ the ratio between the times needed for the same computation is about one-third. For larger N it also becomes much less. One might then ask why we introduced them both. The reason is that important remarks can be made on the grounds of what we just said. Method 2 is certainly to be preferred in the case of scalar computation: there is a factor of almost two in its favor. This is very instructive, because it shows how the ratio between the efficiencies of two different methods can radically change upon passing from a scalar computer to a vector one.

Another consideration pertains to the technique we adopted to optimize the simultaneous computation of M trajectories. This technique is very useful also for computing several trajectories corresponding to different values of the parameter and different initial conditions. Such a case occurs, for instance, when we make a preliminary investigation of the model for a rough sketch of its behavior and we integrate the equations for some more or less large set of parameter values and randomly chosen initial data.

As far as the Broyden method is concerned, a comment has to be made. The search of a periodic orbit with this method requires only one computation of W_k, in contrast to the Newton method, which implies as many computations as the iterations (four, on an average, to reach the precision we desire). Hence, Broyden's method, although it converges more slowly and each iteration involves the computation of $\mathbf{\Phi}^{\tau_k}(\mathbf{x}_k)$, allows a considerable saving of computational time. To be precise, however, we must add a further consideration which partially reduces the advantages of the Broyden method. Once a periodic orbit γ has been determined with a desired accuracy, we are interested in studying its stability properties. To do this, we need the Jacobian of the Poincaré map associated with γ, which means the matrix $W(T)$ computed along γ. Obviously the sequence $\{W_k\}$ converges to $W(T)$, but $\{B_k\}$ does not. An extra computation is then necessary to obtain $W(T)$.

Finally, we use a fourth-order Runge–Kutta method, with a time step in most cases equal to 0.002, to integrate numerically Eq. (A.1) and the associated equation (A.5). The accuracy σ required for the closure of a periodic orbit is 10^{-5}.

ACCKNOWLEDGMENTS

We thank Prof. Mauro Boni for directing us to the quasi-Newton methods and Dr. Anna Maria Baracchi for performing some preliminary numerical experiments. We also acknowledge the Centro di Calcolo dell'Università di Modena for providing computer facilities. This work was supported in part by CNR grant 85.02633.01 and in part by M.P.I.

REFERENCES

1. E. N. Lorenz, *J. Atmos. Sci.* **20**:130–141 (1963).
2. J. H. Curry, *Commun. Math. Phys.* **60**:193–204 (1978).
3. H. Yahata, *Prog. Theor. Phys.* **69**:396–402 (1983).
4. L. N. Da Costa, E. Knobloch, and N. O. Weiss, *J. Fluid Mech.* **109**:25–43 (1981).
5. C. Boldrighini and V. Franceschini, *Commun. Math. Phys.* **64**:159–170 (1979).
6. S. A. Orszag and L. C. Kells, *J. Fluid Mech.* **96**:159–205 (1980).
7. M. E. Brachet, D. I. Meiron, S. A. Orszag, B. G. Nickel, R. H. Morf, and U. Frisch, *J. Fluid Mech.* **130**:411–452 (1983).
8. E. K. Maschke and B. Saramito, *Phys. Scripta* **T2/2**:410–417 (1982).
9. G. Riela, *J. Stat. Phys.* **41**:201–224 (1985).
10. V. Franceschini, C. Tebaldi, and F. Zironi, *J. Stat. Phys.* **35**:317–329 (1984).
11. V. Franceschini and C. Tebaldi, *Meccanica* **20**:207–230 (1985).
12. V. Franceschini, *Phys. Fluids* **26**:443–447 (1983).
13. C. Foias, O. Manley, R. Temam, and Y. M. Treve, *Phys. Rev. Lett.* **50**:1031–1034 (1983).
14. E. K. Maschke and B. Saramito, *Phys. Lett.* **88A**:154–156 (1982).
15. G. Iooss and D. D. Joseph, *Elementary Stability and Bifurcation Theory* (Springer-Verlag, New York, 1980).
16. V. Franceschini, in *Coupled Nonlinear Oscillators* (North-Holland, Amsterdam, 1983), pp. 21–29.
17. V. Franceschini, in *Applications of Mathematics in Technology* (B. G. Teubner, Stuttgart, 1984).
18. J. E. Dennis, Jr., and J. J. Moré, *Siam Rev.* **19**:46–89 (1977).
19. C. Giberti, Thesis, University of Modena (1985).
20. V. Arnold, *Equations Differentielles Ordinaires* (MIR, Moscow, 1974).